A Study of Propagation Effects in a Wireless Test Bed

ALBERT A. LYSKO, and DAVID L. JOHNSON
Meraka Institute / AAIICT (Advanced African Institute for ICT)
Council for Scientific and Industrial Research (CSIR)
Building 43, Meiring Naude Rd, Brummeria 0001, Pretoria
SOUTH AFRICA
{alysko,djohnson}@csir.co.za,   http://www.meraka.org.za/

Abstract: - The paper discusses several effects influencing the propagation in a laboratory wireless test bed, and also aspects important for designing and setting up the wireless test bed with space constraints. A numerical electromagnetic model for the full scale 7×7 wireless mesh network test-bed is discussed. The model includes the coupling and diffraction effects, and is based on the method of moments. The results of numerical simulations are validated with microwave, antenna and received signal strength (RSSI) measurements. The methodology developed for the Wi-Fi card based measurements and relying on the RSSI values is also discussed. The findings from the simulations help to quantify errors and provide grounds for suggestions towards improving design of test-beds.

Key-Words: - electromagnetic propagation, wireless mesh network, wireless sensor network, wireless test-bed, wireless laboratory.

1 Introduction

A wireless network test bed is a group of computers that are able to communicate with each other wirelessly and intended as a test platform for experimental work with various new communication protocols. There are a number of wireless test beds around the globe. Perhaps the most well known examples are CUWin [1], Orbit [2], Roof Net [3] and Kansei [4]. Some of the test-beds were spontaneous and established as a collective effort of independent individuals (e.g. MIT RoofNet), and some were set up by organizations.

These test beds emulate larger wireless networks and are used to develop, test and evaluate new routing protocols for wireless multi-hop mesh networks (WMN). It may also be added that wireless sensor networks (WSN) are often modelled using similar set-ups [4], [10].

The Wireless Africa group of the Meraka Institute seeks innovative solutions to provide wireless broadband Internet access to rural areas in Africa [5], and uses the indoor laboratory test-bed it has established to evaluate and compare various wireless protocols [6], [7].

It should be mentioned that, in modelling complex wireless networks, one may choose to use network simulators like NS2 [8]. Such simulators use simplified models for both networking and physical layers, often leading to inconsistent results [9], and requiring a validation [10], [11]. Under these circumstances, a laboratory test on real-world

equipment provides a solution with more realistic results.

Protocols designed for relatively large communication distances typical in African rural areas, able to utilize the information about the signal level and possibly direction of arrival are typically based on an assumption of propagation close to the log-distance path loss model [12] or on a simple Friis free-space loss equation [12].

The validity of the latter equation is determined by the absence of obstructions, a sufficient distance between nodes, and polarization match [12], [22]. The validity of the former equation adds a requirement of uniformity in the obstacle's profile, and also on the independence of the source on the surroundings.

These factors play an important role in the ability to predict the propagation characteristics [12], [13]. When applied to the results obtained from the test bed simulations, the ability to understand and control the propagation determines the scalability of the simulation outputs [10], and thus the applicability to real-world scenarios.

The propagation aspects in a wireless network are usually modelled with the path loss exponent propagation model, associated with the Rayleigh or Rice fading model [12]. For more complex scenarios, the ray tracing technique [14] is required, since this approximation can provide reliable results for many complex long-range configurations. More accurate numerical methods such as the method of moments [18], [22] are typically used for modelling

particular local effects [15], [16], since these methods often require significant computational resources.

In this work an accurate numerical method for solving electromagnetic coupling problems is applied to the test bed of Meraka Institute. The method is called the method of moments and is described in, for example, [17] and [18]. To the best knowledge of the authors, an investigation of this scale and detail applied to a full-scale wireless network test-bed has not been done before. For example, the authors of paper [19] use the method of moments (MoM) to estimate the radiation pattern for an antenna mounted on a casing of a WSN mote/node. In another paper by Dandekar and Heath [20], the MoM was used to show that in the case of smart antennas, accurate modelling of channel capacity requires a detailed knowledge of the inter-antenna coupling effects.

The findings of this paper aim to help in quantifying the errors in the simulations, and pave a way to suggest improvements to the test bed set-up.

This paper is an extended invited version of the conference publication [21], and is structured in the following way. Section 2 describes the physical layout, main features and electromagnetic characteristics of the test-bed. The Fresnel zone and plane wave formation criteria are then applied to the test bed of the Meraka Institute. This and the results are discussed in Section 3. Section 4 includes the process of building up a full scale model of the test bed, and validation of the model. This is followed by examining the results of a numerical electromagnetic simulation of the resultant full scale model. Section 5 is concerned with the RSSI measurements and is completed with a comparison between the model and received signal strength (RSSI) measurements. The paper is concluded with a discussion and a summary.

2 Description of Test-Bed

The laboratory test-bed of the Meraka Institute is configured as a square 7 by 7 grid of small PCs networked together. Figure 1 shows an overview of the set up, installed in a 6 m by 12 m room. All nodes are equipped with an Ethernet interface for controlling the network, and also with at least one wireless interface for running experiments.

Each PC is equipped with a wireless network card and a 5 dB omnidirectional antenna, and shown in Figure 2.
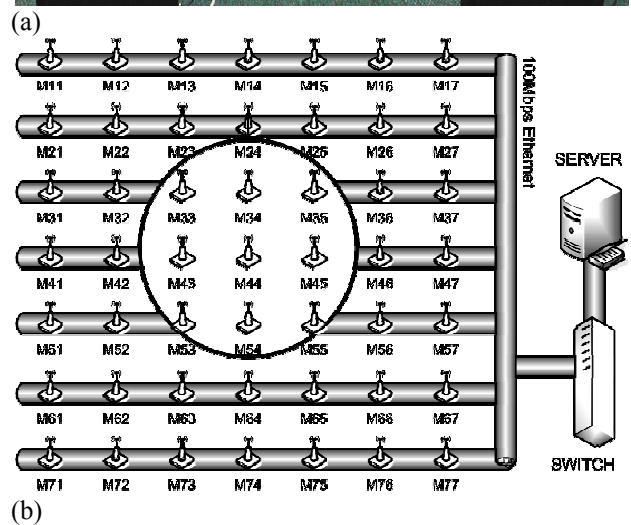

(a)

(b)

Figure 1. (a) Wireless mesh network test-bed. Only 10 out of 49 nodes are shown. Nodes are arranged in a rectangular grid and spaced 0.8 m from one another. (b) A schematic overview of the geometrical set-up, numbering and wired network used for the control purposes (the view excludes the power control lines and auxiliary equipment).

The antennas are connected to respective adapters via 30 dB attenuators. This effectively limits the maximum communication range at the lowest speed (of 1 Mbps) from 17 km to 17 m. The restriction on the communication range permits localization of the experiments to within the room where the test bed is set up. In addition, the 30 dB attenuation helps to reduce the amount of external interference.

A summary of the system parameters relevant to the propagation and transmitter power control is shown in Table I.

Table I. System Parameters (per Node)

Parameter	Value
Wireless network interface card (Atheros chipset) output power	0 to +20 dBm
Sensitivity at 1Mbps	-95 dBm
Antenna gain	5 dBi
Fixed attenuator	30 dB

The laboratory test bed at the Meraka Institute may be compared with, for example, the Orbit mesh laboratory [2]. Both test beds were set up as a dedicated facility. This enhances reproducibility of the results. The Orbit test bed has two large grids of size similar to Meraka's. The Orbit laboratory uses Atheros wireless chipset that supports 802.11 protocols, as does Meraka. The key difference between the Meraka's and Orbit's laboratories is the way they limit the communication range. In the Orbit's wireless test bed, the noise floor is raised by adding white Gaussian noise. Meraka's laboratory uses attenuators.
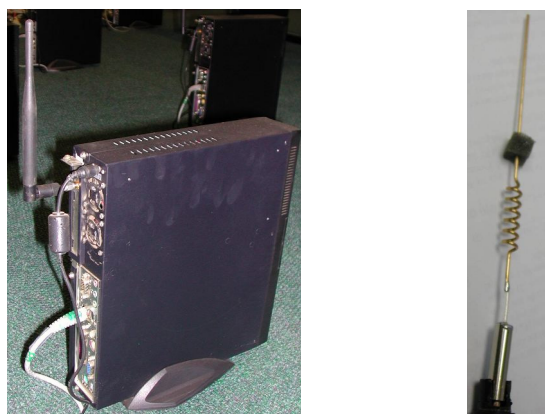

(a)   (b)

Figure 2. (a) View of a single node. The PC case is 30 cm tall, 27 cm long, and 6.3 cm wide. Antenna is 14 cm long and is spaced 3.5 cm away from the PC case. (b) Inside the antenna.

Theoretically, the usage of attenuators lowers the tolerance to the external noise (by 30 dB in the present scenario), as compared to the approach chosen by Orbit. However, the level of the interference penetrating the walls of the laboratory is low and very tolerable in most of the experiments.

At this point, it may also be mentioned that the set-up used by the Meraka Institute may potentially be extended by an injection of a traffic-generated noise. Although this option has not yet been tested, this may be done by setting selected nodes to transmit random sequences, equivalent to a "correlated"

noise. The power distribution of such noise can then also be controlled by an appropriate selection of node positions for the nodes used in the noise generation.

3   Dimensions and Related Effects

The Introduction mentions several physical phenomena contributing to the wave propagation in the test bed. This Section quantifies the effects specifically for the geometry used in Wireless Africa's test bed.

3.1   On Formation of a Plane Wave

The distance between nodes is 0.8 m. This distance is dictated by the need to model free space propagation, where the propagating waves are sufficiently close to plane waves. This requires that the distance between antennas R is much larger than both (a) the wavelength λ, and (b) the product of the antenna's physical size, D, and the respective electrical size D/λ, as per [22]. The restriction (b) is on the maximum phase error (herein 22.5°) and may be written as $R \gg 2D^2/\lambda$. At the lower 2.5 GHz wireless fidelity (Wi-Fi) bands, the wavelength is 12 cm. The antenna has a length of about 14 cm, and the PC case is 30 cm tall. It is easy to calculate that a spacing of 0.8 m is sufficient if the antenna alone is considered.

Figure 2a shows the closeness and asymmetry in mounting of the antenna with respect to the PC case. Thus, if the total height of the structure including antenna and PC case are 40 cm, this may now also be interpreted as D. In this case, the minimum required distance should be over 2.5m.

As it is shown in the subsections following, the proximity of a PC case does influence the radiated field. It would be better (especially at higher Wi-Fi bands) to have the inter-node spacing larger than 0.8 m. In practice the choice has unfortunately been limited by the ability to fit all the nodes within the space available.

Figure 3 depicts a set of plots that illustrate how the minimum recommended spacing between the nodes depends on the physical size of the structure for several commonly used frequency ranges. From the plots, it is clear that in order to be able to increase the density of nodes in a test bed, it is important to keep the physical size of the antenna to a minimum. It may also be noted that the principles of electromagnetic radiation place certain fundamental restrictions on the minimum usable size of an antenna [22].
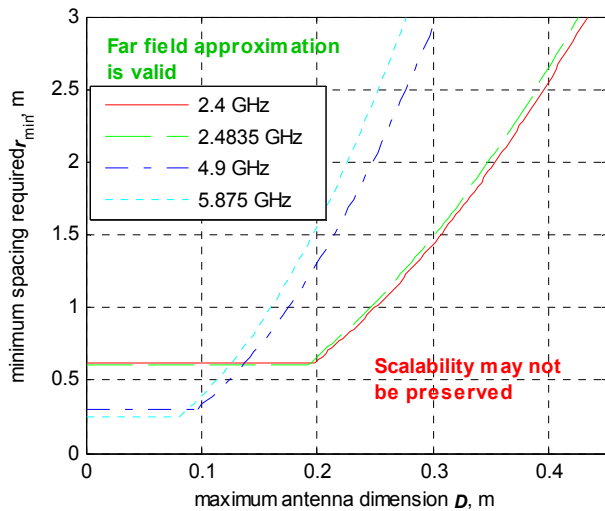
Figure 3. The minimum distance between nodes r_{min}, required to satisfy far field zone approximation, at various frequencies. Horizontal part corresponds to the condition for small antennas: $r_{min} \gg \lambda$ (in this plot $r_{min} > 5\lambda$), whilst bigger antennas require additional spacing, thus leading to $r_{min} \gg 2D^2/\lambda$.

3.2   On Diffraction Effects

The current set up permits for a limited field of view between antennas of different nodes, especially highly pronounced for the nodes distanced by more than 0.8 m. The clearness of the field of view may be expressed with the concept of the Fresnel zone radius [12]. A Fresnel zone is an elliptical volume whose axis on the direct (line-of-sight) propagation path between a transmitter and receiver. The radius of this zone versus position on the line-of-sight path is given by

$$F_1 = \sqrt{n\lambda \frac{d_1 d_2}{d_1 + d_2}} \;,$$

where λ is the wavelength, and $d_{1,2}$ are the distances from transmitter and receiver antennas to an observation point on the line-of-sight, so that d_1+d_2 is the line-of-sight distance between the antennas. The parameter n is the zone number. In practice [12], a rule-of-thumb of minimizing the diffraction effects is to ensure that at least 60% of the 1st Fresnel zone should be clear.

Figure 4 shows results of calculations for the distances typical in the set-up under consideration.

In particular, the maximum radius r_n of the n-th zone (in the middle between 2 antennas) may be written as $r_n = \sqrt{n\lambda R/4}$. This means that at the frequency

2.5 GHz, the 1st Fresnel zone has a 0.45 m radius, measured with respect to the centres of the radiating structure. The radiating structure includes antennae but, where an antenna is in the proximity of metallic structures (such as a PC case), these structures alters the radiation, and should also be taken into account. Presently, as it may be seen in Figure 2a, the centres of the antennas are physically less than 4 cm (a quarter of a wavelength at 2.4 GHz) above the PC cases. The antenna's feed point is even lower. This means that the PC cases must produce diffraction effects. In addition, the PC case is expected to produce near-field effects (such as altering the radiation pattern), since the distance of 3 cm is less than a third of the wavelength.
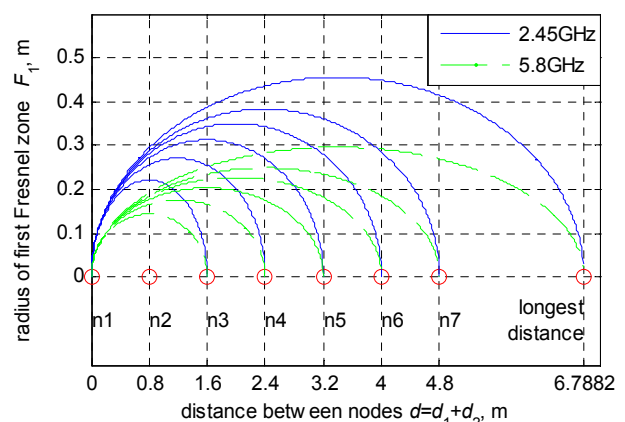

Figure 4. Boundary of the 1st Fresnel zone versus various distances for several combinations of pairs of nodes (from the node 1 at the border of the array to various other nodes).

4   Numerical EM Simulation

A numerical model for electromagnetic (EM) simulations was prepared in several steps, with a state-of-the-art modelling package WIPL-D [17]. Each step was confirmed by measurements. The theory behind the method of moments used in WIPL-D to do the calculations is comprehensively described in [18].

The preparation was started with a model of the physical antenna shown in Figure 2b. The quality of the numerical model was validated by comparing the return loss and radiation pattern against respective values obtained via microwave measurements.

In order to improve the understanding of the effects of arraying, a linear and then square arrays of these antennas in free space were simulated numerically.

Next, a combined model of the antenna together with the PC case was prepared, as shown in Figure

5b. Both the return loss and radiation pattern for the physical setup shown in Figure 2a were measured. This model of PC case with antenna was then used to compile a full-scale model of the test bed. A part of the actual set-up is shown in Figure 1a, and the resulting model is shown in Figure 5c.

4.1 Note On the Output of Simulations and Measurements

All single frequency simulations were done at the frequency of 2.45 GHz that is in the middle of the lower Wi-Fi band.

In all models, the network scattering (S-) parameters [24] were estimated. In this text they have the meaning of and referred to as *coupling coefficients*. A more formal definition used in microwave and antenna testing terminology [24] is as follows.

Each node has a port where the antenna is connected to. It was assumed that the port is well matched on the side of the wireless card (as seen by the antenna). The scattering matrix elements of the respective antenna ports in the test bed, $[S_{ij}]$, are then defined as per [24]:

$$S_{ij} = \frac{V_i^-}{V_j^+}\bigg|_{V_k^+ = 0 \; for \; k \neq j} \quad ,$$

where V_k^+ is the amplitude of the voltage wave incident on port k (port of the antenna at k^{th} node) and V_n^- is the amplitude of the voltage wave reflected from port n (port of the antenna at n^{th} node), while the incident waves on all ports except the jth port are set to zero. Effectively, S_{ij}, is the transmission (or coupling) coefficient from port j to port i when all other ports are terminated in matched loads.

In practice, the latter condition of a termination with a matched load was assumed to be equivalent to respective radios having radio frequency (RF) front-end simply turned off.

It was also assumed that the values $[S_{ij}]$ may be obtained from the received signal strength indicator (RSSI) values, as discussed in Appendix I. The RSSI value is then read at the node (i) receiving the signal, whilst only one node number (j) is permitted to transmit at a time (the remaining nodes are kept silent by turning their radios off).

4.2 Model of Antenna

As a first step, a model of the antenna without a PC case was made, as shown in Figure 5a.

The geometry of this model was made to match the physical antenna shown in Figure 2b. The model was made under the thin-wire approximation [18], [22]. A delta-gap generator model [18] was used as a source/port.

The radiation pattern produced by the numerical model was compared against the measured pattern. The measurements for the physical antenna shown in Figure 2b were done in an anechoic chamber.
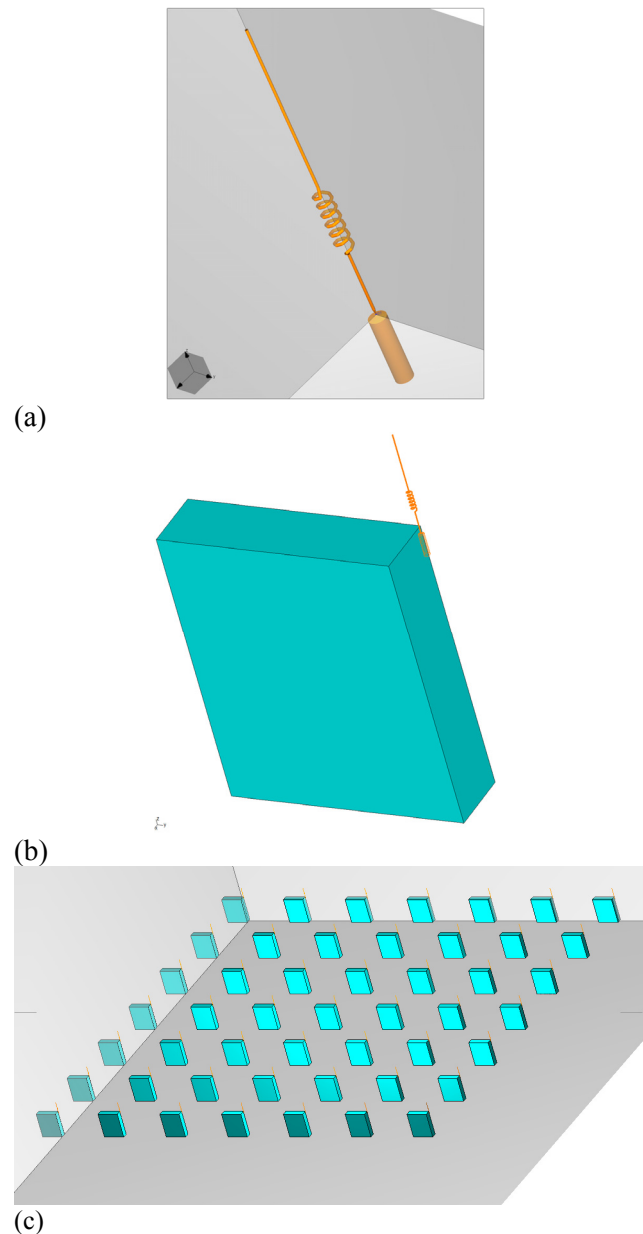

(a)

(b)

(c)

Figure 5. Steps in building a numerical electromagnetic model: (a) Wire model of antenna. The feed point is at the junction of a thick conical wire with the thin wire. (b) Model of a PC case with an antenna. (c) Complete model of the 7×7 network.

In the horizontal plane, the simulated radiation pattern is very close to an ideal omni-directional pattern. Only small deviations from the omni-directional pattern were observed. These deviations are due to the asymmetry introduced by the terminals of antenna's matching coil.

In the vertical plane, that is the E-plane for this antenna, the radiation pattern resembles that of a dipole. A comparison of the simulated and measured normalized patterns in this plane is shown in Figure 6. The modelled and measured patterns match well.

The angular shift between measured and simulated patterns is attributed to the field disturbance created by the pole used for mounting and rotating the antenna during the test.
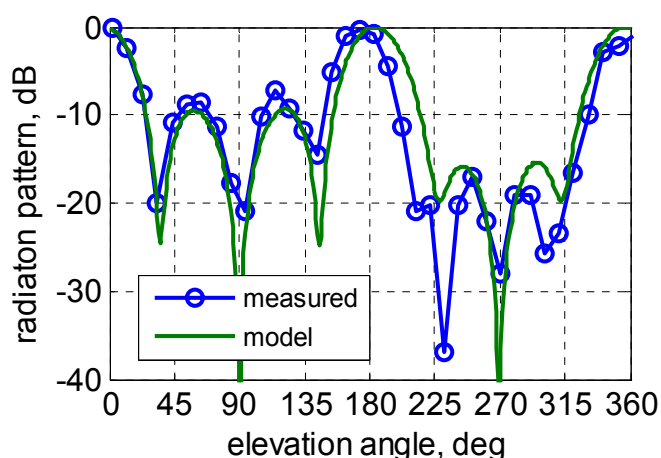

Figure 6. Measured and modelled radiation patterns for the dipole antenna without a PC case.

4.3 Linear and Square Arrays of Antennas

Placing several antennas into an array introduces spatial disturbance for the propagation. This has the form of a periodic structure. It was expected that the arraying of antennas may affect the propagation.

First array model was that of a 7×1 linear array of antennas without PC case. A linear array is a one dimensional structure and is expected to have a simpler set of effects on the propagation, as compared to a two dimensional array.

The modelling has shown that the coupling between the antennas in such a 7×1 linear array is hardly different from the free space loss (FSL) model applied to a single (isolated) antenna. The maximum absolute error was found to be below 0.3 dB.

Second model of arraying was that of a square 7×7 array of the antennas, again with no PC case. This model showed that the propagation was disturbed significantly. A maximum absolute difference between FSL formula and simulation results was

reaching 3 dB.

It was also noted that in both scenarios, the arraying effect was usually minimal for the coupling between the neighbouring elements.

4.4 Combining an Antenna with a PC Case

In the next step, the PC case shown in Figure 2b was approximated with a rectangular box made of a perfect conductor. The antenna was placed in accordance with the physical geometry, transferring the physical structure of Figure 2b into the model shown in Figure 5b.

The numerical electromagnetic modelling of this structure has shown that the radiation pattern produced in the horizontal plane is not close to omni-directional any more. The deviation from the omni-directional pattern was found to be of up to 1.5 dB. This deviation is along the direction of the PC case, and is therefore considered as caused by the PC case.

The measurements done in the anechoic chamber confirmed that the radiation pattern of the antenna attached to a PC case is substantially different from the omni-directional shape. The measured absolute deviation from an omni-directional pattern was as high as 4.5 dB (at the position of a null). The measured and modelled patterns have similar features and profile. The difference in the magnitude of deviation between measurement and simulation is attributed to two factors. These are a simplified model of antenna mounting, and also some error in positioning the antenna with respect to the PC case that was made in the numerical model. It is expected that the combined effect of the imperfectness in the numerical model may have soften the diffraction effects, especially for the direction along the PC case.

4.5 Linear Arrays of PCs

In this intermediate step, two types of linear arrays were modelled to identify the differences in propagation along rows and columns of the physical test bed, and also to see the difference with respect to the effects discussed in subsection 4.3.

The distance between the centres of the PC cases was, as before, kept 0.8 m, the same as in the actual test-bed.

4.5.1 Modelling One Row of the Test Bed

The first scenario is shown in Figure 7a, where the PC cases were oriented to correspond to a single row of the test-bed's grid.

A close look at the simulation results, shown in Figure 7b, reveals that the attenuation of the signal between equally spaced nodes is depends on the position in the array. This effect is particularly pronounced comparing the edges (first and last nodes) of the array against the middle of the array. The maximum difference is equals 1.7 dB. This value is the difference in the coupling of the nodes 4 (middle) and 7 (edge) and the nodes 4 and 1. In terms of the scattering matrix elements, the element $S_{47}=S_{74}$ is compared against the element $S_{41}=S_{14}$.
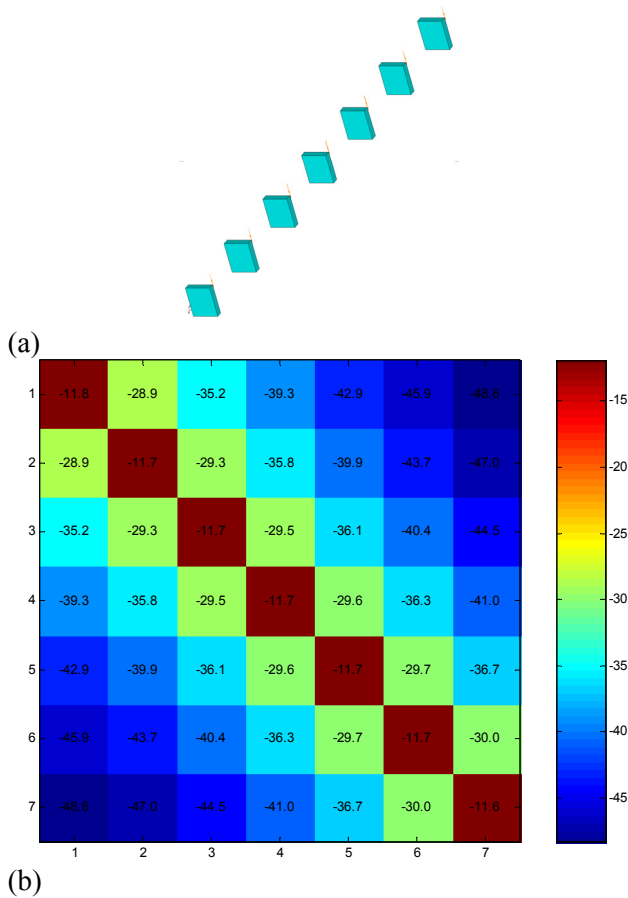

(a)

(b)

Figure 7. Linear array of PCs placed with wide sides parallel to each other. (a) Geometry overview. (b) Coupling level (in dB) between antennas in the array. Indexes along the horizontal and vertical axes correspond to the position of the respective PC in the array.

The difference in coupling between the first and last elements, i.e. $S_{12}=S_{21}$ and $S_{76}=S_{67}$, is attributed to the asymmetry in the placement of the antenna with respect to the PC case (as may be noted in Figure 2b, the antenna is mounted to one side of the PC case, and not to the middle of the PC case).
The same effects, although in a reduced scale, applies to the other elements of the array.

4.5.2   Modelling One Column of the Test Bed

The second scenario is shown in Figure 8. The PC cases in this model were oriented to correspond to a single column of the grid of the physical test bed.
Many of the remarks made in respect of a row of the grid the earlier in this subsection apply to the coupling between the different elements of the array depending on their positions.
Comparing the two scenarios, it is possible to observe that the second scenario shows up to 1.3 dB less attenuation at small distances (within one or two hops between nodes). For larger distances, the second scenario introduces a marginally larger attenuation (up to 0.4 dB).
It should however be noted that a more accurate numerical model should show a stronger attenuation at large distances.
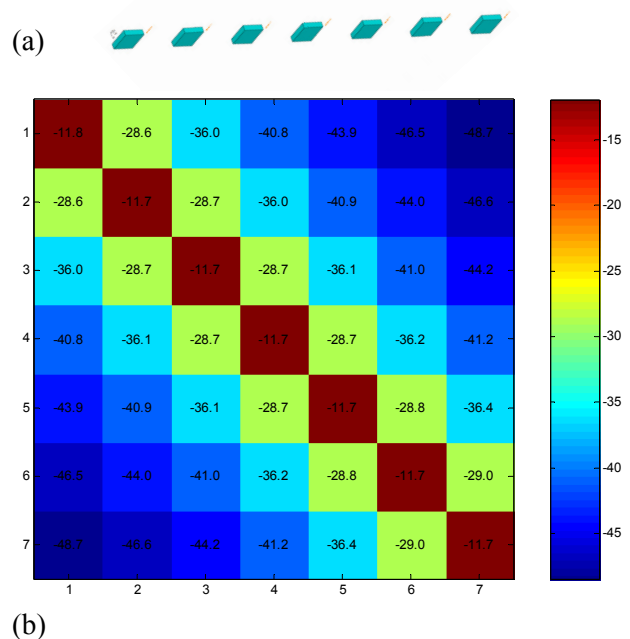

(a)

(b)

Figure 8. Linear array of PCs placed with wide sides along the same line. (a) Geometry overview. (b) Coupling level (in dB) between antennas in the array. Indexes along the horizontal and vertical axes correspond to the position of the respective PC in the array.

Summarising, the results confirm the expectation that the propagation characteristics along rows and along columns of the test bed grid are slightly different.
The two scenarios may also be compared against the linear array of antennas, that was discussed earlier, in subsection 4.3. The comparison shows that the

complexity added by PC cases increases the difference between the predictions due to the FSL equation and the actual attenuation in a linear array of antennas mounted onto PC cases by 2 dB.

4.6 Complete Full Scale Model

A model of the complete 7×7 grid of PCs with attached antennas is shown in Figure 5c. It is based on the template already described in subsection 4.4. That model was placed on a rectangular grid with spacing of 0.8 m.

The nodes are numbered 11, 12, … , 76, 77, where the first digit denotes the horizontal position (row), and the second digit denotes the vertical position (column) in the grid. The node 11 is the most top-left node in Figure 5c (at the origin).

At the simulation frequency of 2.45 GHz, the resulting complete model of the wireless mesh network with 49 nodes translates into an equivalent area of nearly 1000 square wavelengths. This is an electrically large structure. It required approximately 20,000 unknowns using higher-order basis functions [17]. The run time for WIPL-D Pro v.6.1 was 5 hours on a Pentium D 3GHz.

4.6.1 Results

The results of the electromagnetic simulations may be represented as an intensity plot for each of the PCs with relation to all other PCs (nodes). This is shown in Figure 9. There, the most top-left subplot shows the coupling between the node 11 and all the other nodes. The other subplots correspond to the coupling between the respective nodes and all of the remaining nodes. The unit of the colour-bar is dB. The colour-bar was normalized to have 0 dB correspond to the sensitivity threshold of the wireless cards used in the test bed.

Asymmetries present in the radial distribution seen in Figure 9 for each node reveal that, in the test-bed under evaluation, the ability of nodes to communicate with each other does not only depend on the direct line-of-sight distance, as predicted by the log-distance path loss model [12], but also on the angle and position.

The effect may also be observed in a combined intensity plot shown in Figure 10. This figure shows power-averaged results summarizing Figure 9. The averaging was done by adding the relative powers from all plots in Figure 9, where the transmitting node is always placed at the centre of Figure 10.

If the propagation in the test bed was as predicted by the free space equation or by a slightly more complex path loss exponent propagation model, the

intensity plot shown in Figure 10 would have been symmetrical with respect to its centre and decayed monotonically away from the centre. As it may be seen, this is not the case.
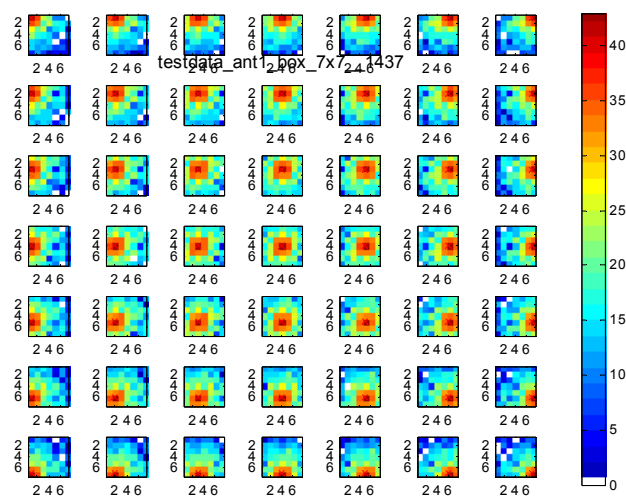

Figure 9. Strength of coupling (relative; in dB) between each node and all other nodes. For example, the coupling of the node 11 and all other nodes is on the most top-left intensity plot. White blocks stand for levels below the sensitivity/communication threshold.
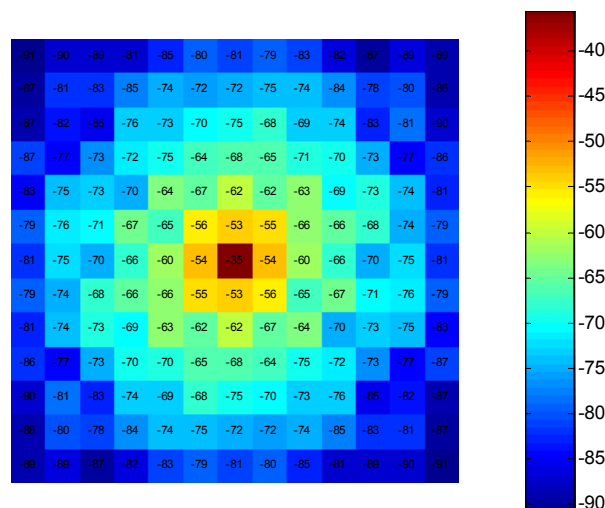

Figure 10. Intensity plot (dB) of the average coupling coefficient per node's relative position (that is taken with respect to the rest of the nodes).

Summarising, the presentation of the data shown in Figure 9 and Figure 10 highlights the following important features: (a) attenuation is not radial, (b) there are nodes with no connection, and (c) propagation in the test bed depends on direction.

The simulation results presented in this section, in particular the data shown in Figure 9, can already be used for estimating an expected coupling between any two nodes in the test-bed under consideration.

Unfortunately, the intensity plots serve well to give a qualitative overview for large datasets, but may be difficult to use for a more qualitative analysis.

In the following subsections, the estimation of the error boundaries achievable in the experiments is discussed.

4.6.2   Comparison against FSL

Figure 11 shows the averaged signal strength against the distance between communicating pairs of nodes. The variation between the extreme (maximum and minimum) values in Figure 11 shows that the signal strength measured around a circle of a fixed radius is not constant as predicted by the FSL formula. The plot shows that the variation may reach 7 dB for an array of antennas without PC cases, and up to 14 dB in presence of PC cases. The standard deviations of the extreme ranges were calculated as 2.6 dB and 7.3 dB, respectively.
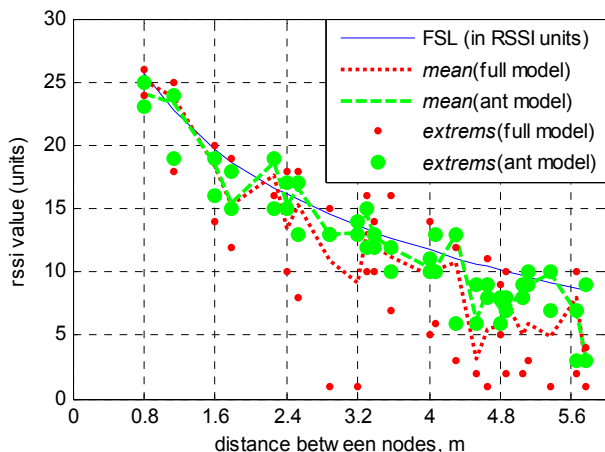

Figure 11. Equivalent signal strength (*RSSI*) versus distance between antennas for a square 7×7 array, modelled numerically. *FSL* indicates the calculated free space loss. *Extremes* denote the maximum and minimum signal strength found for each distance. *Ant model* refers to bare antennas, without the PC case, whilst the *full model* includes the PC cases.

4.6.3   Comparison of Distributions

A distribution of the signal strength plotted against the signal strength is presented in the form of a histogram, as shown in Figure 12. The two histograms shown there are based on the complete set of values of RSSI from the simulation of the square arrays for all inter-node distances.

A comparison of the tails of the distributions in case of antenna alone and in presence of the PC case shows the following. The distribution for the scenario taking the presence of PC cases into account is smoother (less discrete) due to the higher complexity of propagation conditions, which effectively randomises the distribution. In addition, the tails in Figure 12b have higher level (i.e. the distribution is spread more widely).

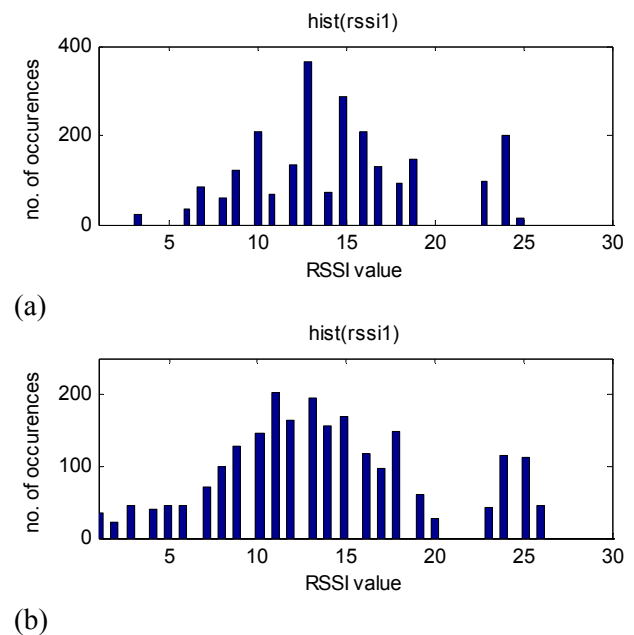These interpretations support the results of the previous subsection.

(a)

(b)

Figure 12. Histogram of the RSSI distribution calculated for a model of dipole antenna (a) *without* the PC case, and (b) *with* the PC case.

5   RSSI Measurements, and Comparison between Measured and Simulated Values of RSSI

This Section is concerned with measurements of the coupling coefficients. It also incorporates a comparison of the results obtained through measurements and numerical electromagnetic analysis.

5.1   Experimental Results

In order to confirm the correctness of the results obtained in Section 4 using numerical modelling, measurements have been made. The measurements rely on the received signal strength indicator (RSSI)

provided by Wi-Fi cards. The measurement methodology, the definitions for the connection matrix, [RSSI], and other terms and parameters of interest used throughout this section are given in Appendix I.

5.1.1 On Observed Difference between RSSI1 and RSSI2

Under the operating conditions in the test bed, the reciprocity principle [22] should be obeyed. This implies that the attenuation experienced by a signal transmitted by node A and received by node B should be the same, as if node B was transmitting and node A receiving. Thus, ideally, the measured connection matrix [RSSI] should be symmetrical with respect to the main diagonal. Thus, the matix element $RSSI_{i,j}$ (termed RSSI1) must be equal to $RSSI_{j,i}$ (termed RSSI2). Measurements have indicated that these values are not always the same. The distribution for this type of variation is shown in Figure 13.
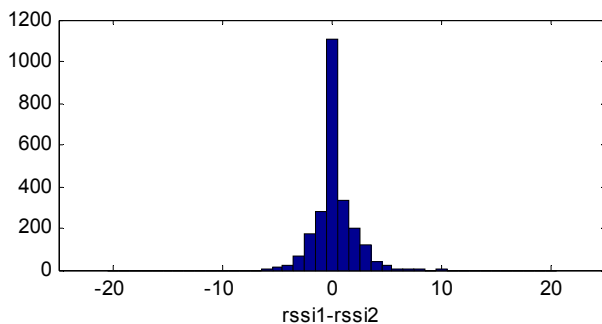

Figure 13. Histogram of the difference between RSSI1 and RSSI2.

The standard deviation of the difference between RSSI1 and RSSI2 was calculated to be 1.6 dB. This value might be considered as a combined measure of the instability in the RF front-end of Wi-Fi cards and due to the external interference.

The difference between the mean values of RSSI1 and RSSI2 was found to be 0.2 dB. This value may indicate the level of external interference. There are two reasons for this conclusion: (a) the selection of transmitting and receiving nodes for a pair is random, and the measurement on each pair was performed more than 2 times, (b) the nearby potential sources of interference such as access points are on one side of the test bed (behind only one wall out of four).

5.1.2 On Observed Time Variation of RSSI

The time variation of the signal was recorded by turning only two nodes *on* (at a time), and recording the RSSI values whilst these nodes were left to exchange the beacons. The rest of the nodes were set to have their transmitters off. A number of such sequences of measurements were made for various combinations of nodes. The mean value for each sequence was subtracted from the data, and the results were then averaged. The results are plotted in Figure 14.
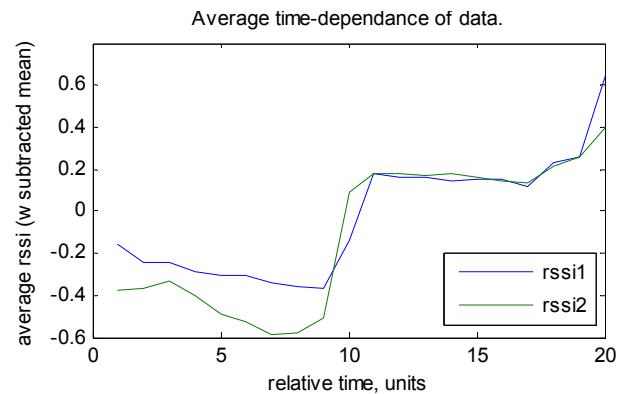

Figure 14. RSSI versus time, measured over period of about 30 seconds, starting from nodes being off. After this interval of time, the change is RSSI was found negligible.

It is clear that there is a slight increase in the signal strength, which is within 1 dB, starting at 10 units of time (after about 10 reading).

This information indicates that in order to keep the test bed measurement consistent, a Wi-Fi card should not be used for more than 5 to 8 consecutive measurements. This was one of the reasons for selecting the random pair-defining approach discussed in subsection I.2 of Appendix I.

It is also possible to observe that the 0.2 dB difference between RSSI1 and RSSI2 reading is present in these measurements as well.

5.1.3 On Distribution of the Measured RSSI values

A histogram of the recorded RSSI values is shown in Figure 15. Its properties bear a good resemblance to the distribution of simulated RSSI values depicted in Figure 12b.

The shape of the measured distribution is even smoother than in the simulated model. This is attributed to the external noise/interference. It may also be attributed to the uncertainty associated with

the manufacturing precision for the RF front-end defining the transmitter's output power level in the in WiFi cards. The stability of the power supplies might have played a role as well.
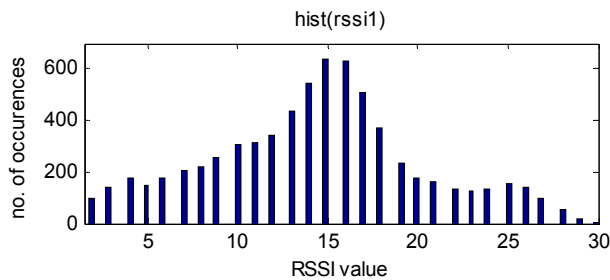

Figure 15. RSSI distribution based on values recorded from tests on the 7×7 test bed.

5.1.4 Note On Parasitic Coupling between Nodes

It was observed that the nodes could sometimes communicate with each other even when the antennas were disconnected and the WiFi card's output ports are terminated with matched loads. The range of this coupling is very limited (typically, no more than 0.5 to 1m), but is significant in the scale of the test bed. This range will be of profound importance, should it become necessary to increase the density of nodes in a test bed.

This parasitic direct coupling is an electromagnetic compatibility (EMC) problem. It depends on the effectiveness of the screening in the WNIC, quality of RF connections, and geometry and quality of the PC case. The PC cases in the test bed under consideration have front panels made of plastic transparent to the RF energy. The rear panels have multiple ventilation holes, also allowing for a RF leakage. The issue is currently being investigated further.

5.2 Comparison between Measured and Simulated Values of RSSI

Figure 16 compares the theoretical (simulated) coupling [S] against the measured values of received signal strength [RSSI]. The former was modelled for two scenarios, with and without the PC case. The data obtained by simulations was brought to the scale of the measured data, i.e. RSSI units, using the simple formula provided in Appendix I. A close correspondence between the measured and simulated sets is observed.

At the shortest distance (between the neighbouring

nodes), where there is no obstruction between the nodes, the result of the full model match the bare antenna model results and also match the respective values recorded from the test bed measurements. This correlates well with the observations made previously in sections 4.3, 4.5, and 4.6.2.

The curves in Figure 16 also serve to assist in ensuring the validity of the numerical EM model versus the measurements done on the test bed.

In addition, the data may be used to determine the expected thresholds of sensitivity for communication between two nodes.
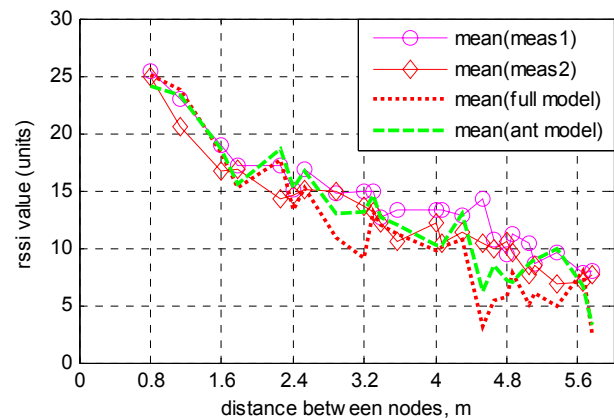

Figure 16. Received signal strength indicator (*RSSI*) value versus distance between nodes - measured (solid lines, *meas1,2*) and simulated results for a rectangular 7x7 test-bed (*model*). *Full* denote the results for the model including PC case, whilst *ant* denotes the simulation for bare antennas. The measurement #1 was done under FreeBSD with output power of 20 dBm. The measurement #2 was done under Linux with output power of 19 dBm.

In order to quantify the effect of the PC cases onto the spread in the RSSI measurements, the standard deviation of RSSI values recorded from all pairs of nodes separated by the same distance was calculated. Figure 17 shows that the measured *average value of standard deviations* for all inter-node distances is around 4 dB. This can be attributed to variation in WNIC output power, sensitivity and array effects, combined. This value may also be used as a simple statistical measure for estimating the variance in channel properties, e.g. for wireless network simulators.

This figure also tells that the same quantity produced by the numerical modelling is lower and depends on the completeness of the model. The

average value of standard deviation is approximately 2 dB and 0.5 dB for the complete model including the PC case (*full*) and for the antenna only model (*ant*), respectively.
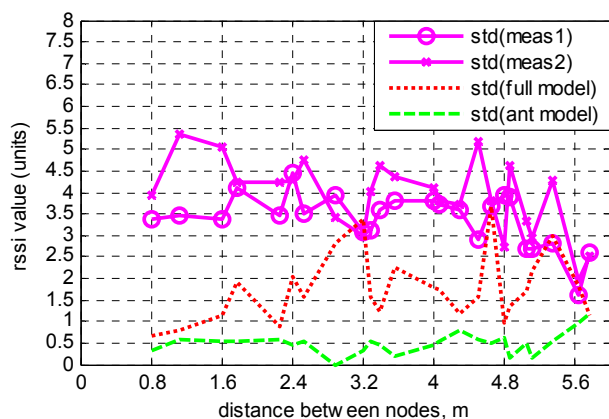

Figure 17. Standard deviation of the sets of RSSI values (for each discrete distance) versus distance. *Meas* refers to values recorded on test bed, and *model* refers to the results obtained from EM modelling. Results of two independent measurements are shown.

The difference between these two values may be interpreted as a possibility to improve the accuracy of RSSI based measurement. This could be done by raising the antennas away from the floor and PC cases, reducing the uncertainty by up to 3 dB (or 1.5 dB on average). Effectively, through simplifying the propagation environment, and making it closer to free space, this would also move the path loss distance exponent closer to 2, the value for the free space.

5.3 Suggestions for Improving Wireless Test Beds

The experience with simulations and measurements done for the test bed of Meraka Institute has permitted to identify of several improvements that could enhance the physical setup of a wireless test bed.

The antenna installation height above the PC cases is to be increased to ensure clearness of the first Fresnel zone. This will help to reduce the unwanted diffraction effects and simplify the characteristics of propagation within the test-bed. This improvement is currently under consideration.

Ideally, the setup should be housed in an anechoic chamber, which can eliminate or reduce the external interference and also reduces self-interference by absorbing the signals produced by the test bed. A minimum outlay could be to screen the surrounding walls at the height of the antennas.

Parasitic coupling may be reduced by selecting PC cases and WNIC's that are well screened. Alternatively, an additional external screening or absorbing material may be employed.

6   Discussion

The results show that, in the present realization of the test bed, the path loss is influenced by the complex diffraction phenomena due to several factors. The main contributors include: (a) the closeness of the antennas to the PC cases, causing strong asymmetry in the horizontal radiation pattern of the antennas; (b) the line-of-sight between the antennas is close to the metallic PC cases, causing angle-dependant diffraction effects (e.g. different for x- and y- axes in the grid, as considered in Section 3.3); (c) array effects due to periodic placement of antennas.

The effects (a) and (b) may be reduced by installing the antennas on sufficiently high non-conducting stands. The minimal height of the stands is defined by the clearness of at least the 1st Fresnel zone (i.e. 0.45 m at 2.45 GHz). This upgrade work is planned at Meraka Institute's laboratory.

The effects of arraying has been estimated by modelling a 7×7 grid of the 0.8 m spaced bare-dipole antennas (without any PC cases or other elements). This model has shown a deviation in the inter-antenna coupling (with respect to the Friis equation) up to +1…-3 dB, with the standard deviation of up to 1.5 dB. The numerical model that includes the PC cases has shown a much greater standard deviation, of up to 3.5 dB. These results indicate that raising antennas, away from the PC cases, may lower the standard deviation by at least 2 dB.

Looking at the pictures provided in some of the above-mentioned research papers (see for example [2]), most of the above conclusions with regards to the effects due to antenna mounting and positioning may also apply to other laboratory wireless test-beds.

7   Summary

The indoor wireless mesh network test bed set up by the Meraka Institute has been considered from the point of view of signal propagation within the test bed.

The estimates for the Fresnel zone and plane wave criterion were applied to verify the propagation conditions in the given configuration.

A full scale numerical electromagnetic model of the test bed was built up. The modelling relied on the accurate moment-method based program WIPL-D Pro, which includes the near field and diffraction effects explicitly.

Each part of the complete model was validated by the relevant microwave and antenna measurements.

The modelling of individual parts of the complete model permitted to identify and quantify several effects, including arraying of antennas, and influence of the PC case on radiation.

The effect of the undesired near field and diffraction phenomena on the inter-node wireless links in the test bed was studied with a full scale numerical electromagnetic model. The numerical modelling has indicated the error boundaries for the results that come out of simulations run on the test bed.

A measurement procedure for capturing the received signal strength indicator (RSSI) values was developed that mimics the microwave measurement of coupling between the nodes. The results obtained for the matrix of RSSI values were compared to the calculated network scattering [S] matrix. It was seen that a good agreement between the measured and calculated values exists.

It was also concluded that it is desired to separate the antennas from the metallic objects such as the PC cases. Such a separation is expected to improve the quality of the results produced by the test bed.

Appendix I – Methodology of Wi-Fi Based Measurements

The measurements of the signal strength on the test bed were made by recording the values of the received signal strength indicator (RSSI) read out of the wireless network interface cards (WNIC-s).

I.1   Obtaining RSSI from 802.11-compatible Wireless Cards

Many wireless cards have a function, which allows viewing the value of Received Signal Strength Indicator (RSSI). RSSI is a measure of the received signal strength (not necessarily the quality) in a wireless environment, in arbitrary units. RSSI is usually used internally in a wireless networking card to determine when the level of signal in the air is below a certain threshold at which point the network card is clear to send (CTS).

RSSI measurements result in a one-byte integer value, varying from 0 to 255 depending on the vendor. A value of 1 will indicate the minimum signal strength detectable by the wireless card, while 0 indicates no signal. The value has a maximum of $RSSI\_Max$. For example, Cisco Systems cards return an RSSI of 0 to 100, reporting 101 distinct power levels. In the case of the test bed under consideration, the $RSSI\_Max$ is 60. The Wi-Fi chipset used in the testbed for the measurements is made by Atheros. An Atheros based card with an RSSI range of 0 to 60 was used for the measurements. It uses a simple formula to convert from RSSI to dBm [26], i.e.

$$power\ level\ (dBm) = RSSI – 95.$$

This gives a power range of –95 to –35 dBm for an RSSI range of 0% to 100%.

RSSI is measured on/by a WNIC every time a beacon is broadcast from another node containing the service Set Identifier (SSID). According to the standard 802.11 [25], RF energy from the antenna is measured from the beginning of the start frame delimiter (SFD) and the end of the PLCP (physical layer convergence procedure) header error check (HEC). This happens periodically, at an interval specified by the user with the default of 100 ms.

Under a Linux operating system, the following command may be used to obtain the RSSI values:

wlanconfig ath0 list sta

where *ath0* is the name of the wireless interface. This command returns a list of all other WNICs within the communication range, together with the respective RSSI values (this is only true for WNICs which are in *Master* or ad-hoc mode, and not WNICs which are in *client* mode).

I.2   Measurement Methodology and Data Presentation

In order to improve the quality of results, only 2 nodes (1 pair) were set to have RF power *on* during each individual measurement. Then only the external interference (dampened by walls) was present. Most of the measurements were done using channel 8, which exhibited a better signal to noise ratio within the Meraka Institute's test bed environment.

It is possible to accelerate running the tests by turning all nodes *on*, and reading RSSI. However, the analysis of data has shown that the RSSI values

recorded in this way were different from the values recorded with the approach described in the previous paragraph. Typically the values were higher by up to 6 dB. At the same time, the signal quality (SQ) indicator read out of the WNICs was lower, typically by about 20 units. These effects are due to mutual interference of 49 nodes communicating or attempting to communicate with one another. This test speed-up opportunity was not considered any further.

As stated before, the 7×7 test bed has a total of 49 nodes. Each of these nodes may be identified with a unique number (e.g. running from 1 to 49). Then, considering the 49 node mesh as a set of pairs, the strengths of connections between the two nodes constituting each pair may be represented by a 49 x 49 matrix, as illustrated in Table II. This *connection matrix* (also referred to as an *RSSI matrix*, [RSSI]), is in many ways similar to the scattering matrix **S** used in microwave theory [24]. Each element in this connection matrix, $RSSI_{ij}$, corresponds to the signal strength recorded by the i–th node due to the signal from j–th node.

The diagonal of the matrix is not a valid entry, because a node cannot transmit to itself.

Table II. Elements of the connection matrix [RSSI]. The elements denoted with "-"cannot be read from a WNIC .

-	$RSSI_{1,2}$	$RSSI_{1,3}$	…	$RSSI_{1,49}$
$RSSI_{2,1}$	-	$RSSI_{2,3}$	…	$RSSI_{2,49}$
$RSSI_{3,1}$	$RSSI_{3,2}$	-	…	$RSSI_{3,49}$
…	…	…	…	…
$RSSI_{49,1}$	$RSSI_{49,2}$	$RSSI_{49,3}$	…	-

The simplest approach to performing the test to find all the coefficients in [RSSI] would have been to have two *for* loops with respect to the first and second indexes for matrix elements $RSSI_{i,j}$, $i,j=1..49$. This would however mean that the transmitters in the WNIC would be working continuously for an excessive period of time (corresponding to testing 48 other nodes), possibly leading to an increase in the temperature of RF front-end, and, thus, some time-dependency of the measured results.

In the test results presented, a random approach for the selection of the nodes for each pair was used. The elements $RSSI_{i,j}$ and $RSSI_{j,i}$ were recoded during the same iteration. In this paper, the respective records are referred to as *RSSI1* and *RSSI2*.

It may be necessary to note that the raw measurement results were processed to remove those values of RSSI that did not belong to the accepted range of values (1-60).

I.3   Translation between RSSI Values and Simulated Data

The simulated scattering matrix parameters [S] may be recomputed into the units of [$RSSI$] and vice versa using the following relationship valid for Atheros based WiFi cards [26]:

$$RSSI_{equiv} = Tx - 2L_{Att} + 20\log_{10}(|S_{ij}|) + 95,$$

where Tx is the output power level (which was kept to 20 dBm for most of the tests), L_{Att} is the value of attenuator before antenna (i.e. 30 dB), S_{ij} is the coupling coefficients (i.e an element of the network scattering matrix), and $RSSI_{equiv}$ is the value of equivalent received signal strength.

In this expression, the coupling coefficients are assumed to be obtained from a simulation and thus already include the influence of the propagation loss, antenna gain and also the mismatch between antenna and WNIC.

References:
[1] *CUWiN - Champaign-Urbana Community Wireless Network.* Available: http://www.cuwireless.net/.
[2] Ganu S., Kremo H., Howard R., and Seskar I., Addressing Repeatability In Wireless Experiments Using ORBIT Testbed, *1st Intl. Conf. on Testbeds and Research Infrastructures for the Development of Networks and Communities* (Tridentcom 2005), 2005.
[3] Aguayo D., Bicket J., Biswas S., De Couto D., MIT Roofnet: Construction of a Community Wireless Network, *Student Oxygen Workshop,*

2003. Available: MIT roofnet website - http://pdos.csail.mit.edu/roofnet/doku.php.

[4] Ertin E., Arora A. et al., Kansei: A Testbed for Sensing at Scale, *The Fifth International Conference on Information Processing in Sensor Networks*, 2006. IPSN 2006.

[5] *Mpumalanga Mesh Network Project*, Web site http://wirelessafrica.meraka.org.za/wiki/index.php/Mpumulanga_Mesh.

[6] Johnson D., Kaka Y., and Hay J., A New Grid Based Test Bed Environment For Carrying Out Ad-Hoc Networking Experiments, *SATNAC conference*, 2006.

[7] Johnson D.L. and Lysko A.A., Comparison of MANET Routing Protocols Using a Scaled Indoor Wireless Grid. *Mobile Networks and Applications*, Vol. 13, No. 1-2, April 2008, Springer Science (Computer Science), 2008, pp. 82-96.

[8] Issariyakul T., and Hossain E., *An Introduction to Network Simulator NS2*. Springer, 410p. To appear in October 2008.

[9] Andel T.R., Yasinac A., On the credibility of MANET simulations. *IEEE Computer Society*, Vol. 39, July 2006, pp. 48–54.

[10] Naik V., Ertin E., Zhang H., Arora A., Wireless Testbed Bonsai, *The 4th International Symposium on Modeling and Optimization in Mobile, Ad Hoc and Wireless Networks*, 2006. pp. 1-9.

[11] Lucio G.F., Paredes-Farrera M., Jammeh F., Reed M.J., OPNET modeler and NS-2 - Comparing the accuracy of network simulators for packet-level analysis using a network testbed. *WSEAS Transactions on Computers*, Vol. 2, No. 3., Jul 2003, pp. 700-707.

[12] Rappaport T.S., *Wireless Communications: Principles and Practice*, 2nd Ed., Prentice Hall, 2002.

[13] Bulusu N. et al., Effects of Detail in Wireless Network Simulation, *SCS Communication Networks and Distributed Systems Modeling and Simulation Conference*. USC/ISI TR-2000-523. September, 2000.

[14] Schoonen A., Designing Wireless Indoor Radio Systems with Ray Tracing Simulators. *Technical report, Eindhoven University of Technology*, Dec.2003. Available: http://people.spacelabs.nl/~admar/SimpleCSD/report.pdf.

[15] Suzuki H., Tran T. V. A., and Collings I. B., Characteristics of MIMO-OFDM Channels in Indoor Environments. *EURASIP Journal on Wireless Communications and Networking*, Vol.

2007, Article ID 19728, Hindawi Publishing Corporation.

[16] Roelens L., Joseph W., and Martens L., Characterization Of the Path Loss Near Flat and Layered Biological Tissue for Narrowband Wireless Body Area Networks. *In: International Workshop on Wearable and Implantable Body Sensor Networks*. 2006; Cambridge, USA. pp.50-53

[17] Kolundzija B. et al., *WIPL-D Pro v6.1: 3D Electromagnetic Solver, Professional Edition. User's Manual*, WIPL-D d.o.o., 2006.

[18] Kolundzija B. and Djordjevic A., *Electromagnetic Modeling of Composite Metallic and Dielectric Structures*, Artech House, 2002.

[19] Su W. and Alzagha M., Channel Propagation Measurement and Simulation of MICAz mote, *WSEAS Trans. on Computers*, Issue 4, Vol. 7, Apr 200,. pp. 259-264.

[20] Dandekar K. R., Heath R. W., Jr., Physical layer characterization of smart-antenna equipped mobile ad-hoc network nodes in an urban environment, *IEEE Military Communications Conference, MILCOM 2003*. Vol. 2, Issue 13-16 Oct. 2003, pp. 1376 – 1381.

[21] Lysko A.A., Johnson D.L., A Numerical Study of Propagation Effects in a Wireless Mesh Test Bed, *Proceedings of the 6th WSEAS Int. Conf. on Applied Electromagnetics, Wireless and Optical Communications (Electroscience'08)*, 2008, pp. 41-46.

[22] Balanis C.A., *Antenna Theory: Analysis and Design*. 3rd Ed., Wiley-Interscience, 2005.

[23] McLean J.S., A Re-Examination of the Fundamental Limits on the Radiation Q of Electrically Small Antennas, *IEEE Trans. Antennas Propagat.*, Vol. 44, No. 5, May 1996, pp. 672-676.

[24] Pozar D., *Microwave Engineering*, 3rd Ed., Wiley, 2004.

[25] Standard 802.11: Wireless LAN Medium Access Control (MAC) and Physical Layer (PHY) Specifications, 1999 Edition (R2003).

[26] Converting Signal Strength to dBm Values, white paper, Available on-line at: http://www.wildpackets.com/elements/whitepapers/Converting_Signal_strength.pdf.